REVIEW ARTICLE

Asian Research Association

INTERNATIONAL RESEARCH JOURNAL OF MULTIDISCIPLINARY TECHNOVATION

DOI:10.54392/irjmt2253

The Ultimate Load of the Fiber-Reinforced Concrete Slab Foundations Subjected the Concentrated Load by ANSYS

Dang-Bao Tran [1,2] *, Radim Cajka [1]

[1] Department of Structures, Faculty of Civil Engineering, VSB–Technical University of Ostrava, Ludvíka Podéště 1875/17, Ostrava-70800, Czechia.

[2] Department of Civil Engineering, Faculty of Architecture, Thu Dau Mot University, Tran Van On 06, Binh Duong Province-75000, Vietnam

* Corresponding author email: dang.bao.tran@vsb.cz ; baotd@tdmu.edu.vn

DOI: https://doi.org/10.54392/irjmt2253

Received: 06-04-2022; Revised: 22-09-2022; Accepted: 24-09-2022; Published: 30-09-2022

Abstract: In practice, the slab foundation is used widely in civil engineering. Besides the concrete material, fiber concrete is applied more popular in the slab foundations. Determining the ultimate load of the slab foundations is a complex problem due to the relation of the soil-structure interaction (SSI) problem, which depends on both the structures and the subsoil characteristics. ANSYS is a finite element software which is a reliable and effective technique to simulate the structure model. This paper aims to determine the ultimate load of the fiber-reinforced concrete slab on the ground subjected to the concentrated load by ANSYS software. The nonlinear material of the structure and the subsoil will be considered in this work. The validation test of the numerical model will be through the experiment data. This study has shown that the numerical model is reliable for the structure design.

Keywords: ANSYS 2020 R1, Fiber Concrete, Finite Element Method, Soil-Structure Interaction

1. Introduction

In practice, the slab foundation is used widely in civil engineering. Soil-Structure Interaction (SSI) is the research about the interaction i) between the foundation and the subsoil and ii) between the structure and the foundation. Many scientists studied the theoretical and experiments on the slab interaction with the subsoil, including with the concrete material and fiber concrete applied more popular in slab foundations [1-12].

Numerical modeling has a significant role in capturing the natural behavior of the SSI. Determining the ultimate load of the slab on the ground is a complex problem due to the relation the SSI, which depend on both the structures and the subsoil characteristics [13, 14]. The commercial structural software (SCIA, SAP2000, ETABS), which subsoil is represented by the simple spring model (Winkler or Pasternak), cannot express the actual behavior of soil [15, 16]. Meanwhile, the geotechnical software (MIDAS GTX NX, PLAXIS), which has many subsoil model options, is straightforward in the foundation structure model [17].

ANSYS software was used for modeling slabs on the ground with many degrees, from the simplification assumption to the complex model [18-20]. However, the ultimate load values did not mention in these papers. Numerical modeling by ATENA software was performed [21-22] based on an experimental work [12], in which the mechanic parameters were determined by the specialized laboratory test. Yet, the subsoil is assumed by linear elastic, which is not actual behavior.

This paper aims to determine the ultimate load of the fiber-reinforced concrete slab on the ground subjected to the concentrated load by ANSYS software. The nonlinear material of the structure and the subsoil are considered in this work. The validation test of the numerical model will be through the experiment data and numerical method performed by [12, 22].

2. Specification of Analyzed Structures

Three fiber reinforced-concrete square slabs with a side length, 2 m, and a thickness of 0.15 m, executed for SSI experimental in, were chosen to perform the numerical model by ANSYS 2020R1 software [12]. The concentrated force was applied to the slabs through the square plate with a side length, 0.4 m and a thickness of 0.03 m.

Table 1 summarizes the fiber concrete mechanic properties of three slabs. The steel reinforcement 8, with the strength characteristics shown in Table 2, was distributed with the distance a = 0.1 m in each direction. The concrete cover of the bar was set to 30 mm. The subsoil under the slab foundations, qualified as sandy clay CS, is a depth of ten meters [17]. The strength characteristics of the subsoil are shown in Table 3.

Table 1. Mechanic properties of fiber concrete

Slab	Fiber [kg/m3]	Compressive strength (cylinder)		Tensile strength	
		Mean compressive strength [MPa]	Standard deviation [MPa]	Mean tensile strength [MPa]	Standard deviation [MPa]
G02	25	29.28	0.846	2.96	0.223
G03	50	25.27	2.012	3.12	0.21
G04	75	24.90	1.007	3.17	0.593

Table 2. Strength characteristics of reinforcement

Modulus of elasticity [MPa]	Poisson's coefficient	Yield strength [MPa]	Tensile strength [MPa]	□lim	k
20 x 104	0.2	550	577.5	0.025	1.05

Table 3. Strength characteristics of the subsoil

Unit weight [kN/m3]	Modulus of deformability [MPa]	Poisson's coefficient	Cohension [kPa]	Friction angle [degreee]	Dilatancy angle [degreee]
19	12.5	0.35	9	19.3	0

Figure 1. The typical inspection slab [12]

The ultimate load of three slabs, G02, G03, G04, performed by the experimental, was 542 kN, 640 kN, 752 kN, respectively. Figure. 1 shows the typical inspection slab. One can find the details of the experiment in [12].

3. Analysis model by ANSYS 2020 R1 software

The analyzed structures were modeled by ANSYS software, in which many structural analysis elements are available. The SOLID65 element, derived from the work of William, was used to model the validation slabs [23]. Nine parameters are required for the SOLID65 element. The purpose of this study is to determine the ultimate load; therefore, the values of constant 1, 2, 4 corresponding 0.3, 1, -1, respectively, are set up [24]. The parameter uniaxial tensile cracking stress (3) is defined by Table 1. Other variables (6-9) are assigned zero values.

The main difference between concrete and fiber concrete in compression is the descending or softening of the stress-strain curve [25]. This paper focuses on the ultimate load; therefore, the stress-strain of plain concrete can apply to the fiber concrete. The following equations suggested by MacGregor et al [24, 26]. were used to define the compressive uniaxial stress-strain curve of the fiber concrete.

$$f = \frac{E_c \varepsilon}{1+\left(\frac{\varepsilon}{\varepsilon_0}\right)^2}, \quad (1)$$

$$\varepsilon_0 = 2\frac{f_c'}{E_c}, \quad (2)$$

$$E_c = \frac{f}{\varepsilon}, \quad (3)$$

in which f is the stress of the fiber concrete corresponding to the strain value, ε

f'_c is the compressive strength of the fiber concrete

E_c is the elasticity modulus defined by EC2 [27]

$$E_c = 22\left(\frac{f_{cm}}{10}\right)^{0.3}, \quad (4)$$

where f_{cm} is the mean of the compressive strength of the specimens. Figure. 2 depicts the compressive uniaxial stress-strain curve of the fiber concrete material of the slab G02.

The LINK8 element was used to model the reinforcement in the tested slabs. The bond between the concrete and steel was supposed to be perfect. The bilinear stress-strain with hardening for the steel derived from EC2 standards was selected for the material model of the reinforcement bars [27]. The SOLID186 element was chosen to model the subsoil and load plate. Linear stress-strain of steel is assigned for load plate.

From a geological view, the subsoil is not complicated. Therefore Drucker-Prager model, which is the adjustment of Von Mises model comprising the impact of hydrostatic pressure on yielding, is chosen to capture the actual behavior of the subsoil [28]. The subsoil is modeled by inhomogeneous, divided into five layers with a thickness of 400 mm space [18, 29-31]. The three dimensions of the subsoil model are 6000 x 6000 x 2000 mm. The boundary condition selected in this paper is fixed all surfaces except the layer contact with the slab [22]. The modulus of deformability, E, and Poisson's coefficient, μ, changed with the depth is shown in Table 4, which is calculated by the formulas in [32].

$$E(z) = E_{def}(1 + m_1 z), \quad (5)$$

$$\mu(z) = \mu(1 + m_2 z), \quad (6)$$

in which m_1 = 0.5065, m_2 = 0.0123

z is the depth of the soil (m).

For the comparison, the modulus of deformability of the soil is selected with three variants, E_top, E_mid, E_bot, which are denoted for the three positions, top, middle, and bottom layer of the solid soil element, respectively. The element CONTA174 with TARGE170 is used to model the interaction between the foundation and subsoil. The friction between the foundation and subsoil is neglected. The non-linear analysis was performed by an incremental load process applying the Newton–Raphson method. The tolerance error is assigned with the value, 5%.

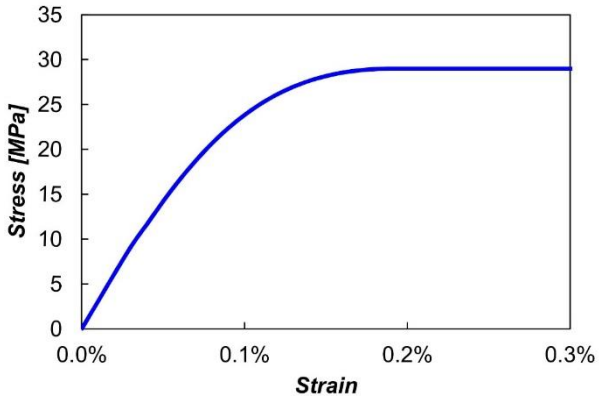

Figure 2. The stress-strain of the fiber concrete of the slab G02

Table 4. The modulus of deformability and Poisson's coefficient of the subsoil layers

The depth of the subsoil [m]	The modulus of deformability of the subsoil layers E [MPa]	Poisson's coefficient μ
0	12.5	0.350
0.2	13.8	0.351
0.4	15.0	0.352
0.6	16.3	0.353
0.8	17.6	0.353
1	18.8	0.354
1.2	20.1	0.355
1.4	21.4	0.356
1.6	22.6	0.357
1.8	23.9	0.358
2.0	25.2	0.359

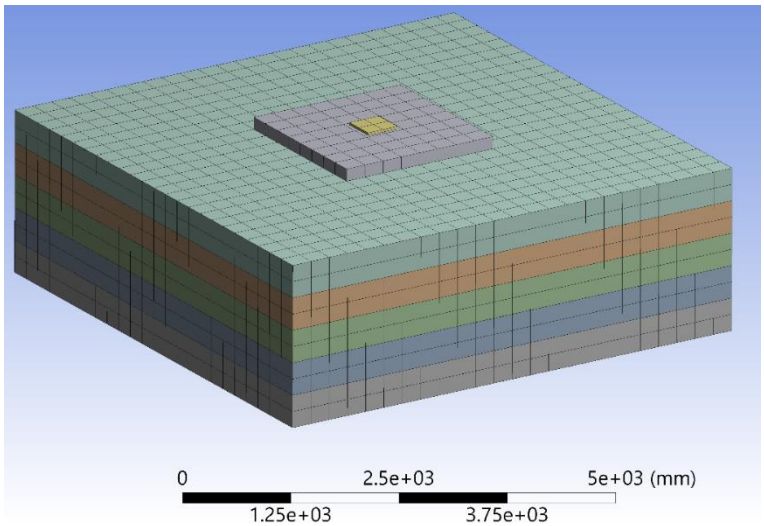

Figure 3. 3D numerical model by ANSYS 2020 R1 of the analyzed structures

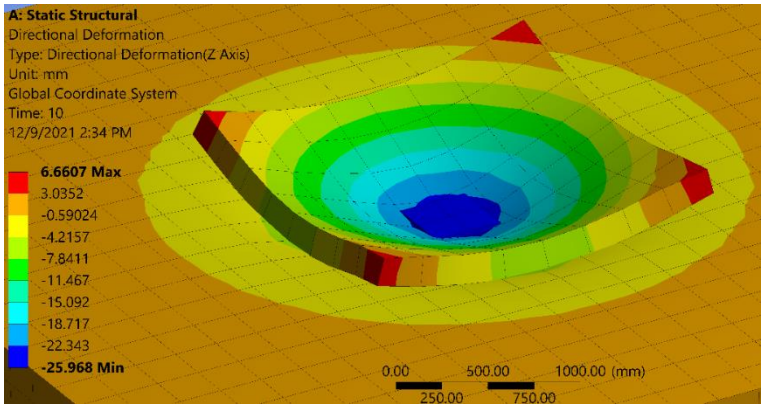

Figure 4. Vertical displacement of the slab G02 corresponding with E_top at the load P = 536.8 kN

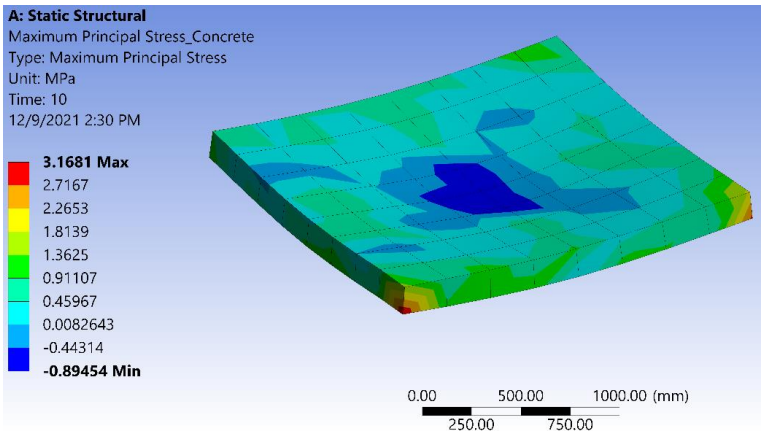

Figure 5. The principal tensile stress of the concrete of the slab G02 corresponding with E_top at P = 536.8 kN

Figure. 3 shows the model of the slab foundation and the inhomogeneous subsoil performed in ANSYS 2020 R1.

4. Result discussions

In this section, the results obtained by ANSYS simulation are presented and compared with the results of i) the experiment, ii) numerical model by ATENA software performed by with three variants modulus of deformability subsoil, E = 12.5, 22.5, and 32.5 MPa [12,22].

Figure. 4 shows the 3D deformation of the slab G02 corresponding with E_top at the load P = 536.8 kN. The deformation mode is uniform with the experimental, where the corners of the slab are moved to the ground [12, 17]. Figure. 5 and Figure. 6 depict the principal tensile stress of the concrete and the tensile stress of the reinforcement of the slab G02 corresponding with E_top at the load P = 536.8 kN, respectively. It can be seen

from Figure. 5 and Figure. 6 that the tensile stress of the concrete passed over the stress limit, and the tensile stress of the reinforcement reached the yield strength.

Figure. 7 and Figure. 8 show the deformation of the subsoil and the slab at the section plane through the center of slab G02, respectively. The deviation of settlement at the center of the slab and the subsoil is 4.99%.

Figure. 9, Figure. 10, and Figure. 11 show the deflection of the slab G02, G03, G04, respectively, under ultimate load at the section plane through the sensors (4 to 8) performed by experimental [12] and ANSYS-E_top. From Figure. 9 to Figure. 10, it can be seen that the numerical model can estimate the maximum deflection accurately; the deflection curve of the slab foundation derived from the numerical model is more outstretched than the actual deflection.

In Table 5, the ultimate load of the ANSYS with three variants is presented and compared by the deviation with the experimental data of three slabs [12]. Figure. 12 and Figure. 13 show the load-displacement diagram of slab G02, G03 respectively. The comparison results were performed between i) ANSYS simulation, ii) experiment data, and iii) ATENA software [12, 22]. It can be observed that the ultimate load of the ANSYS (E_top) is close to the experimental data.

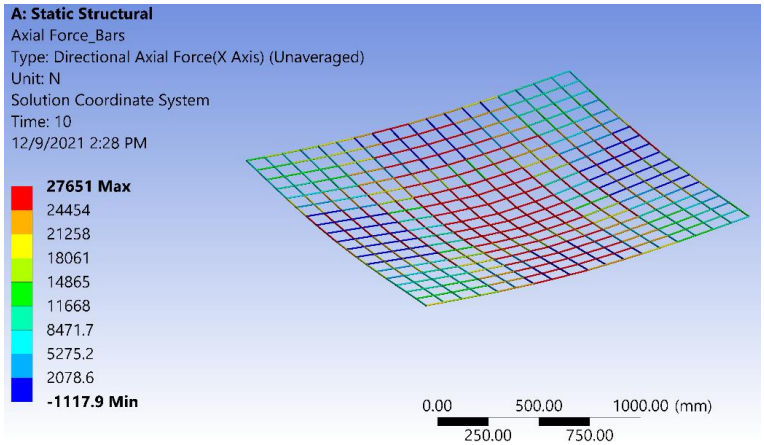

Figure 6. The tensile stress of the reinforcement of the slab G02 corresponding with E_top at P = 536.8 kN

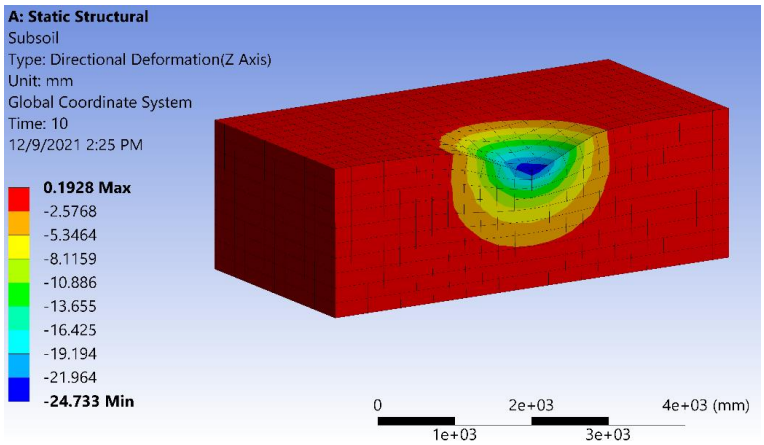

Figure 7. The deformation of the subsoil at the section plane through the slab center of slab G02

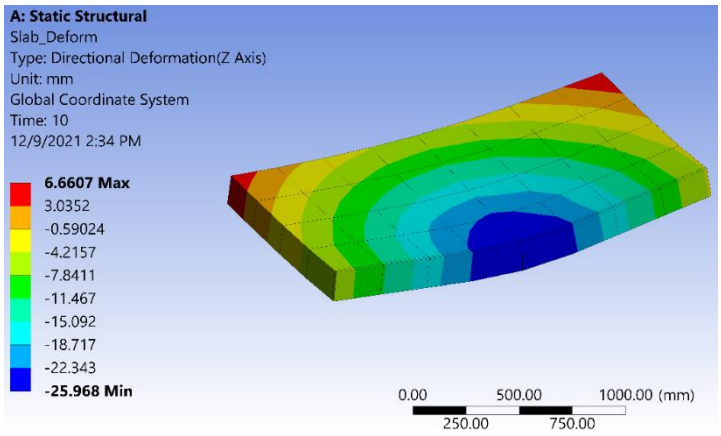

Figure 8. The deformation of the slab at the section plane through the slab center of slab G02

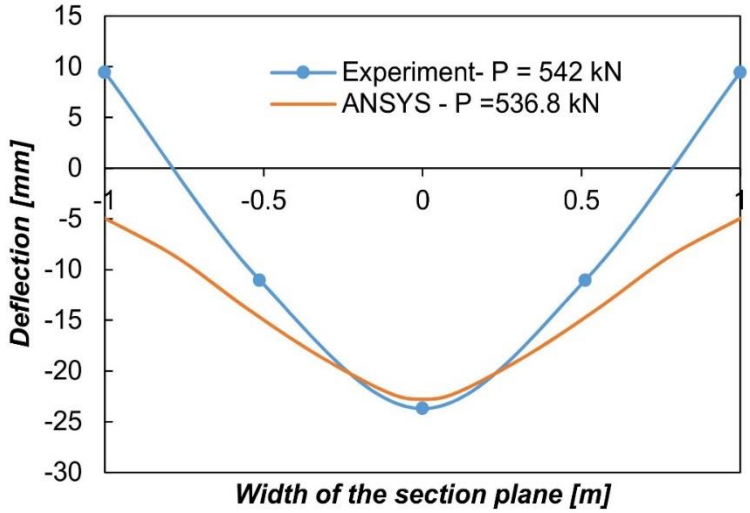

Figure 9. The deflection of the slab G02 at the section plane through the sensors (4 to 8) derived from experimental and ANSYS

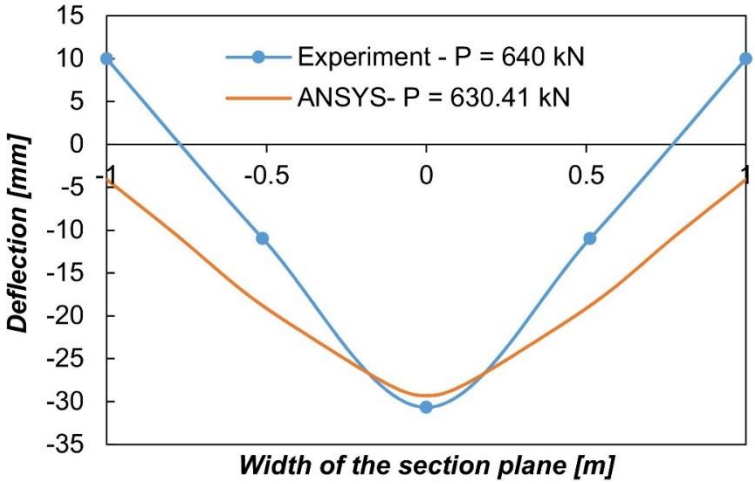

Figure 10. The deflection of the slab G03 at the section plane through the sensors (4 to 8) derived from experimental and ANSYS

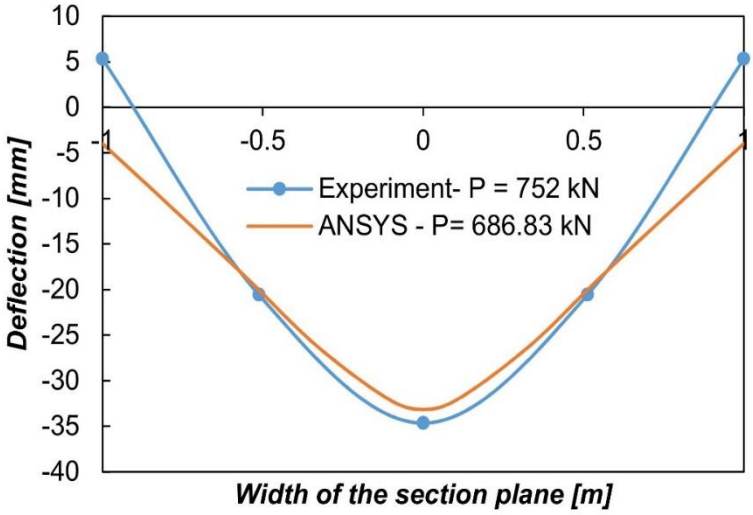

Figure 11. The deflection of the slab G04 at the section plane through the sensors (4 to 8) derived from experimental and ANSYS

Table 5. Comparison the ultimate load between the methods

Slabs	Experimental [kN]	E_top		E_mid		E_bot	
		P [kN]	Deviation %	P [kN]	Deviation %	P [kN]	Deviation %
G02	542	536.8	0.96	586.11	8.14	615.5	13.56
G03	640	630.41	1.49	671.03	4.85	708.7	10.73
G04	752	686.83	8.67	725.3	3.55	762.6	1.41

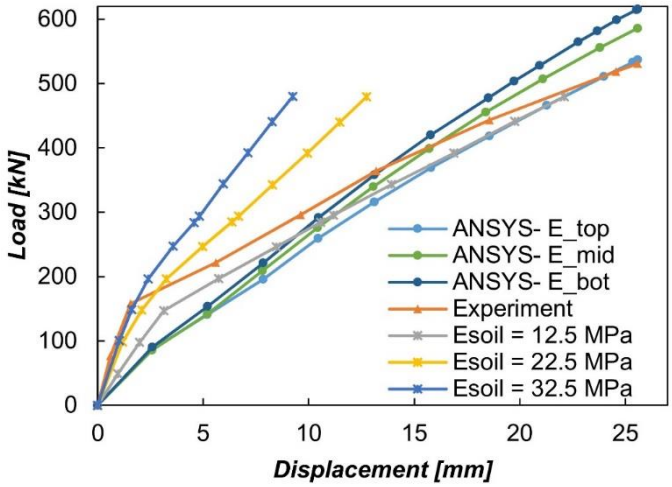

Figure 12. The load-displacement of slab G02 derived from the methods

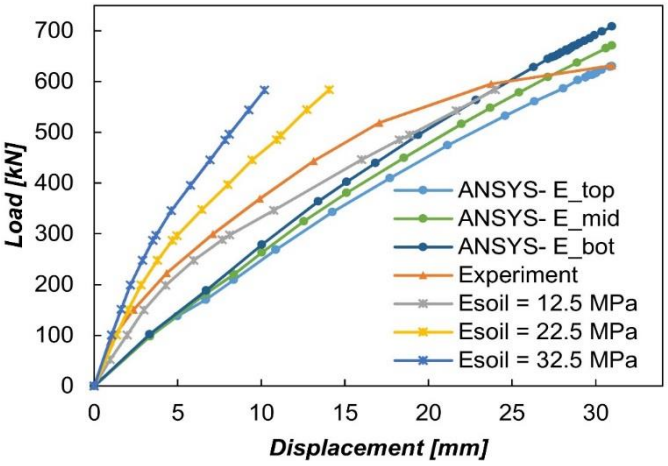

Figure 13. The load-displacement of slab G03 derived from the methods

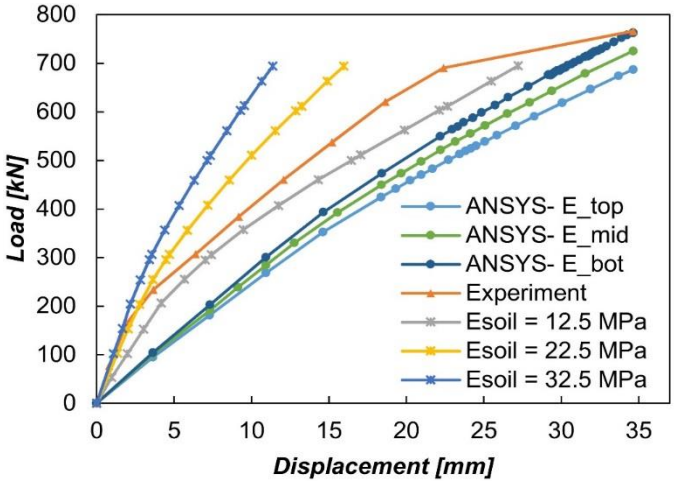

Figure 14. The load-displacement of slab G04 derived from the methods

In Figure. 14, the load-displacement diagram of slab G04 is depicted for i) ANSYS simulation, ii) experiment data, and iii) ATENA software [12, 22]. It can be seen that the ultimate load of the ANSYS (E_bot) is close to the experimental data. From Figure. 12 to Figure. 14, one can see that the increase of the modulus of deformability values leads to a rise to the ultimate load in ANSYS simulation. It is worthy to note that the ultimate loads of slab fiber concrete obtained by [22] tend to be higher than those of the experimental [12].

5. Conclusion

In this work, the ultimate load of the fiber-reinforced concrete slab on the ground subjected to the concentrated load was performed and compared with the experiment data and ATENA software. Some conclusions can be withdrawn:

1. The modulus of the deformability significantly influences the load capacity of the slab foundation.
2. ANSYS simulation can express the subsoil model, for example, Drucker-Prager, which cannot perform in ATENA software.
3. The stress-strain of the plain concrete can be applied to the fiber concrete to predict the slab foundation's ultimate load.
4. It can be seen from Figure. 12 to Figure. 14 that the ultimate loads of fiber-reinforced concrete slab obtained by ATENA software tend to be higher than those of the experimental. It can lead to unsafety in design.
5. The deviation of ANSYS simulation (E_top) and the experimental ranges (0.96-8.67%). The ultimate loads of fiber-reinforced concrete slabs obtained by the numerical model in this study underestimate the experimental results acceptance range.
6. The numerical method can estimate the maximum deflection of the slab accurately; the deflection curve of the slab foundation derived from the numerical method is more outstretched than the actual deflection.

References

[1] L.G. Sorelli, A. Meda, & G.A. Plizzari, Steel Fiber Concrete Slabs on Ground: A Structural Matter, ACI Structural Journal, 103 (2006) 551-558. [DOI]

[2] S. Chen, Strength of steel fibre reinforced concrete ground slabs, Proceedings of the Institution of Civil Engineers-Structures and Buildings, 157 (2002) 157-163. [DOI]

[3] L. Pazdera, R. Cajka, L. Topolář, P. Mateckova, V. Bilek, O. Sucharda, Measurement and Utilization of Acoustic Emission for the Analysis and Monitoring of Concrete Slabs on the Subsoil, Periodica Polytechnica Civil Engineering, 63 (2019) 608-620. [DOI]

[4] A. Alani, D. Beckett, & F. Khosrowshahi, Mechanical Behaviour of a Steel Fibre Reinforced Concrete Ground Slab, Magazine of Concrete Research, 64 (2012) 593-604. [DOI]

[5] H. Falkner, Z. Huang, & M. Teutsch, Comparative Study of Plain and Steel Fiber Reinforced Concrete Ground Slabs, Concrete International, 17 (1995) 45-51.

[6] X. Huang, X. Liang, M. Liang, M. Deng, A. Zhu, Y. Xu & X. Wang, Experimental and theoretical studies on interaction of beam and slab for cast-in-situ reinforced concrete floor structure, Jianzhu Jiegou Xuebao (Journal of Building Structures), 34 (2013) 63-71.

[7] D. Kueres, M. Ricker, J. Hegger, Improved Shear Reinforcement for Footings—Maximum Punching Strength, ACI Structural Journal, 115 (2018) 1365-1377. [DOI]

[8] L.C. Hoang, A. Pop, Punching shear capacity of reinforced concrete slabs with headed shear studs, Magazine of Concrete Research, 68 (2016) 118-126. [DOI]

[9] D. Beckett, Ground-supported slabs made from steel-fibre-reinforced concrete: An appraisal of punching shear, Concrete, 38 (2004) 30-31.

[10] A. Meda, G.A. Plizzari, New Design Approach for Steel Fiber-Reinforced Concrete Slabs-on-Ground Based on Fracture Mechanics, Structural Journal, 101 (2004) 298-303. [DOI]

[11] M.A. Miltenberger, E.K. Attiogbe, & B. Bissonnette, Behavior of conventional reinforcement and a steel-polypropylene fiber blend in slabs-on-grade, Materials and structures, 40 (2007) 279-288. [DOI]

[12] R. Cajka, Z. Marcalikova, M. Kozielova, P. Mateckova, & O. Sucharda, Experiments on Fiber Concrete Foundation Slabs in Interaction with the Subsoil, Sustainability, 12 (2020) 3939. [DOI]

[13] P. Pollak, L. Zlatinska, Influence of Subsoil Quality on Design of Slab Foundation, Roczniki Inzynierii Budowlanej, Zeszyt, (2013) 105-110.

[14] D. Tomasovicova, N. Jendzelovsky, Stiffness Analysis of the Subsoil under Industrial Floor. Procedia Engineering, 190 (2017) 365–370. [DOI]

[15] J. Kralik, N. Jendzelovsky, Contact problem of reinforced concrete girder and non-linear winkler foundations, Geomechanics 93, (1994) 233–236.

[16] T.F. Fwa, X.P. Shi, S.A. Tan, Use of Pasternak Foundation Model in Concrete Pavement Analysis, Journal of Transportation Engineering, 122 (1996) 323–328. [DOI]

[17] L. Duris, E. Hrubesova, Numerical Simulation of the Interaction between Fibre Concrete Slab and Subsoil—The Impact of Selected Determining Factors, Sustainability, 12 (2020) 1–17. [DOI]

[18] J. Labudkova, R. Cajka, Comparison of Analysis of Linear Inhomogeneous and Nonlinear Half-Space in Foundation-Subsoil Interaction, International Journal of Mechanics, 10 (2016) 90-98.

[19] J. Vaskova, R. Cajka, 3D Numerical Model of the Subsoil-Structure Interaction and Comparison of the Results with Experimentally Measured Values, Key Engineering Materials, 738 (2017) 298–309. [DOI]

[20] R. Cajka, J. Labudkova, Dependence of deformation of a plate on the subsoil in relation to the parameters of the 3D model, International Journal of Mechanics, 8 (2014) 208–215.

[21] M. Kozielova, Z. Marcalikova, P. Mateckova, & O. Sucharda, Numerical Analysis of Reinforced Concrete Slab with Subsoil, Civil and Environmental Engineering, 16 (2020) 107-118. [DOI]

[22] R. Cajka, Z, Marcalikova, V. Bilek, & O. Sucharda, Numerical Modeling and Analysis of Concrete Slabs in Interaction with Subsoil, Sustainability, 12 (2020) 9868. [DOI]

[23] K.J. Willam, Constitutive model for the triaxial behaviour of concrete, International Association for Bridge and Structural Engineering (IABSE), 19 (1974) 1–30.

[24] A.J. Wolanski, (2004) Flexural Behavior of Reinforced and Prestressed Concrete Beams Using Finite Element Analysis, Master's Theses (1922-2009) Access Restricted to Marquette Campus.

[25] Materials, Fib Model Code for Concrete Structures 2010, John Wiley & Sons, Ltd, (2013) 74–150. [DOI]

[26] J.G. MacGregor, J.K. Wight, S. Teng, P. Irawan, (1997) Reinforced concrete: Mechanics and design, Prentice Hall, Upper Saddle River, New Jersey.

[27] E. Committee, (2005) EN 1992-1-1 Eurocode 2: Design of Concrete Structures—Part 1-1: General Ruels and Rules for Buildings, European Committee, Brussels, Belgium.

[28] D.C. Drucker, W. Prager, Soil mechanics and plastic analysis or limit design, Quarterly of Applied Mathematics, 10 (1952) 157–165. [DOI]

[29] R.K.N.D. Rajapakse, A.P.S. Selvadurai, Response of circular footings and anchor plates in non-homogeneous elastic soils, International Journal for Numerical and Analytical Methods in Geomechanics, 15 (1991) 457–470. [DOI]

[30] R.F. Stark, J.R. Booker, Surface Displacements of a Non-Homogeneous Elastic Half-Space Subjected to Uniform Surface Tractions. Part I: Loading on Arbitrarily Shaped Areas, International Journal for Numerical and Analytical Methods in Geomechanics, 21 (1997) 361–378. [DOI]

[31] J.P. Doherty, A.J. Deeks, Scaled boundary finite-element analysis of a non-homogeneous elastic half-space, International Journal for Numerical Methods in Engineering, 57 (2003) 955–973. [DOI]

[32] F.L. Pan, Effect of buried depth of soil layer on Poisson's ratio and lateral compressive stress to vertical compressive stress ratio, China Civil Engineering Journal, 18 (1985) 53–60.

Acknowledgements

This study has been supported by the Technical University of Ostrava through the funding research of Czech Republic.

Conflict of interest

The Authors have no conflicts of interest to declare that they are relevant to the content of this article.

Does this article screened for similarity?

Yes

About the License